Rapid Communications

Superconductivity in sodalite-like yttrium hydride clathrates

Christoph Heil,[1] Simone di Cataldo,[1] Giovanni B. Bachelet,[2] and Lilia Boeri[2,*]
[1]*Institute of Theoretical and Computational Physics, Graz University of Technology, NAWI Graz, 8010 Graz, Austria*
[2]*Dipartimento di Fisica, Sapienza Università di Roma, 00185 Roma, Italy*

(Received 13 January 2019; revised manuscript received 16 April 2019; published 10 June 2019)

Motivated by the discovery of near-room-temperature superconductivity in the sodalite-like clathrate hydride LaH_{10}, we report *ab initio* calculations of the superconducting properties of two closely related hydrides YH_6 and YH_{10} for which an even higher T_c has been predicted. Using fully anisotropic Migdal-Eliashberg theory with Coulomb corrections, we find almost isotropic superconducting gaps, resulting from a uniform distribution of the coupling over states of both Y and H sublattices. The Coulomb screening is rather weak, resulting in a Morel-Anderson pseudopotential $\mu^* = 0.11$, at odds with claims of unusually large μ^* in lanthanum hydrides. The corresponding critical temperatures at 300 GPa exceed room temperature ($T_c = 290$ and 310 K for YH_6 and YH_{10}), in agreement with a previous isotropic-gap calculation. We estimate anharmonic effects to be weak. The different response of these two compounds to external pressure along with a comparison to low-T_c superconducting YH_3 may inspire strategies to improve the superconducting properties of this class of hydrides.

DOI: 10.1103/PhysRevB.99.220502

The report of near room-temperature superconductivity with a superconducting critical temperature (T_c) of 265 K in the lanthanum superhydride LaH_{10} at 190 GPa [1–4] set a new record for superconductivity only three years after another superhydride SH_3 opened up the high-pressure route to conventional high-T_c superconductivity [5,6]. These breakthroughs stem from two seminal papers of Ashcroft, who first conjectured that high-T_c conventional superconductivity would arise in high-pressure elemental metallic hydrogen [7] and later proposed that the huge threshold pressure for hydrogen metallization might be significantly reduced in binary hydrogen compounds XH_n by exploiting the additional internal pressure due to the X atoms [8].

Three years of research resulted in the determination of the high-pressure phase diagrams of most binary hydrides [9,10], clarifying that those hydrides which exhibit high-T_c superconductivity mainly fall into two classes: (i) covalent hydrides, such as SH_3 and PH_3, in which H and the other element X form a network of covalent bonds, driven metallic by the high pressure, and (ii) metallic hydrides of alkaline and rare earths, such as LaH_{10}, which form hydrogen-rich sodalite-like clathrates (SLC) with highly symmetric structures [1–3,11–14], whose T_c's are close to, or even higher than, room temperature. In class (i), the chance of high-T_c superconductivity is governed by the degree of covalency of the H-X bonds, and $X = S$ seems to approach a *sweet spot* [6,15–22]; in class (ii), the specific electron-phonon (*e-ph*) mechanism leading to high-T_c has not yet been identified as clearly [23–25].

In a suggestive scenario, LaH_{10} is identified as the first experimental evidence of high-T_c superconductivity in precompressed atomic hydrogen. Following the empirical observation that, in many XH_n binary hydrides the highest T_c's occur when the H-H distance is close to that of atomic hydrogen [9,10,14,26,27], one might postulate that superconductivity in XH_n hydrides is entirely dominated by the dense H sublattice. From this perspective, once the X atoms provide charges to the hydrogen sublattice and stabilize a crystal structure with sufficiently short H-H distances, high-T_c superconductivity should inevitably follow. As we have recently shown, such an oversimplification leads to badly wrong expectations [28,29] since superconductivity strongly depends on crucial details of the electronic structure, which cannot be guessed on the basis of the H-H distances alone. In particular, the prerequisite for high T_c in high-pressure hydrides is a substantial role of hydrogen in the *e-ph* coupling, but the X atom can also play an important role, affecting T_c, anisotropy of the gap, electronic screening, etc.

The aim of this Rapid Communication is to identify the electronic-structure features behind high-T_c superconductivity in SLC hydrides. To this end, we will reexamine two representative high-T_c high-pressure hydrides of this class, YH_6 and YH_{10}, using the fully anisotropic *ab initio* Migdal-Eliashberg (ME) theory as implemented in the EPW code [30–32]. The choice of yttrium hydrides is motivated by two main arguments: (i) Among all predicted SLC rare-earth superconducting hydrides, yttrium hydrides have been predicted to exhibit the highest absolute value of T_c (YH_{10}) and the lowest stabilization pressure (YH_6) [13,14]. (ii) Since, in the Periodic Table, yttrium belongs to the same group as lanthanum, the crystal structures and superconducting properties of its high-pressure hydrides closely track those of the analogous lanthanum compounds [1–4]. In contrast to lanthanum, yttrium has the practical advantage that its f states, problematic for DFT, are way above the Fermi level and play no role in the bonds and bands of its hydrides [24].

Studying yttrium hydrides as prototypical examples of SLC high-T_c superconductors, we thus aim, on one hand, at providing an accurate reference for such materials, exploring a range of parameters where most approximations used in the standard theory of superconductivity, such as the

*lilia.boeri@uniroma1.it

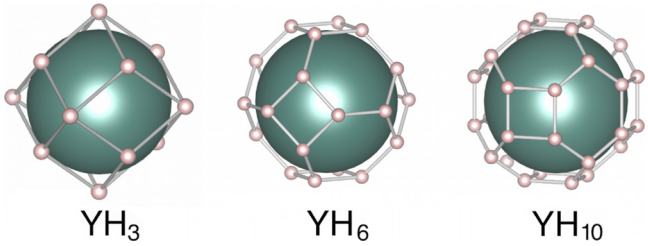

FIG. 1. The fcc YH_3 (left), bcc YH_6 (center), and fcc YH_{10} (right) crystals are lattices of polyhedral hydrogen cages (H = small pink balls) with an yttrium atom in their middle (Y = green balls, drawn with a radius of 1.62 Å, midway between its core and its covalent radius). While the YH_3 and YH_6 cages share all faces, giving rise to a perfect tessellation of space, the YH_{10} cages only share the hexagonal faces. In this picture, the H-H distances correspond to an external pressure of 300 GPa: $d_{HH} = 1.74$ Å for YH_3, $d_{HH} = 1.19$ Å for YH_6, and two slightly different lengths $d_{HH} = 1.03, 1.11$ Å for YH_{10} (see the text).

McMillan-Allen-Dynes formula for T_c and the use of an empirical Coulomb pseudopotential are not guaranteed to hold, and, on the other hand, at identifying a rationale behind the physicochemical ingredients needed to reduce their stabilization pressure without reducing their high T_c. In this spirit, we will not address the thermodynamics of the Y-H system but concentrate on the high-symmetry SLC structures of YH_6 and YH_{10} which, according to previous *ab initio* calculations, are stable with record T_c's of 260 K for YH_6 at 120 GPa, and of 303 K for YH_{10} at 400 GPa [33].

Our results confirm that, in addition to a reasonably short H-H distance, both the superconducting behavior and the dynamical stability under pressure of these YH_n hydrides are determined by the peculiar geometry of such a densely connected H lattice (similar to a *sponge* of H filaments whose cavities are occupied by Y atoms) and not by the chemical details of the enclosed atom.

Figure 1 shows the two high-T_c yttrium hydrides considered in this Rapid Communication [34], YH_6 and YH_{10}, together with the low-T_c YH_3 crystal, experimentally observed above 10 GPa, whose predicted maximum T_c is 40 K at 18 GPa [35,36]. In YH_3 and YH_6, a hydrogen atom sits on each of the 14 (24) vertices of the fcc (bcc) Wigner-Seitz primitive cell; in YH_{10}, it sits on each of the 32 vertices of a chamfered cube. For each such polyhedron, well-known relations connect the length of its edge (the H-H distance d_{HH}), its volume V (proportional to the unit-cell volume of the corresponding crystal), its average radius, etc. For example, $d_{HH} = 0.69V^{1/3}$ in YH_3, $0.45V^{1/3}$ in YH_6, and $0.38V^{1/3}$ in YH_{10}. Geometrical constraints not only control (i) the H-H distance, important for high T_c, but also (ii) the Y-H distance, important for the involvement of Y in the *e-ph* interaction, and (iii) how tight or loose is the host clathrate cavity where the (fixed-size) guest atom sits; which, in turn, triggers the onset of their dynamical instability at low pressure, discussed later [34].

We now focus on the two high-T_c superconductors [37], whose bands (left) and densities of states [(DOS), right] are shown in Fig. 2 for YH_6 (top) and YH_{10} (bottom).

Unless otherwise stated, all subsequent results refer to a pressure of 300 GPa where both YH_6 and YH_{10} are

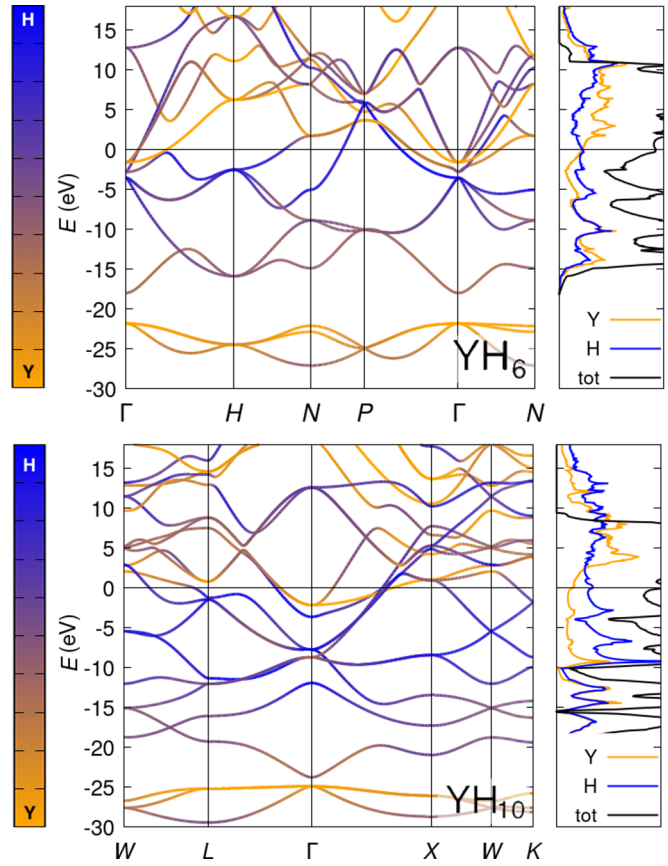

FIG. 2. Left: electronic energy bands where the color gradient indicates the projection onto H (blue) and Y (orange) states. Right: total DOS (black), partial Y DOS (orange), and partial H DOS (blue). Energies are given with respect to E_F. The scale limit for the DOS plots is 0.35 st eV^{-1} $spin^{-1}$.

dynamically stable and their T_c is close to its maximum. The color gradient indicates the projection onto H (blue) and Y (orange) states. In both compounds, the hydrogen-derived bands have a total bandwidth of ∼40 eV. Remarkably, their dispersion over this energy range is well described by quasi-free-electron bands [38] with largest deviations where the H- and Y-derived states significantly hybridize, i.e., ∼25 eV below the Fermi level ($4p$ semicore states) and in a region of ∼10 eV around the Fermi level ($4d$, $5s$ states). The Fermi level cuts the band structure where both H and Y contributions to the electronic structure are sizable: In particular, around the Brillouin zone center (Γ) the bands have mostly Y character, whereas, at its boundaries, they are mostly H [39]. The corresponding Fermi surfaces (FSs) are shown in Fig. 3.

In a superconductor, when two or more orbitals/bands at the Fermi surface couple to phonons with different intraband strengths, an anisotropic superconducting gap $\Delta_{\mathbf{nk}}$ results. Its behavior can be obtained entirely from first principles within the anisotropic ME theory: The anisotropic *e-ph* Eliashberg functions are calculated within the linear-response theory using the Wannier interpolation technique implemented in the EPW code [31,32] and, for the fully screened Coulomb interaction, the *GW* approximation [41,42]. We do this for YH_6 and YH_{10}, showing our result in the right panels of Fig. 3.

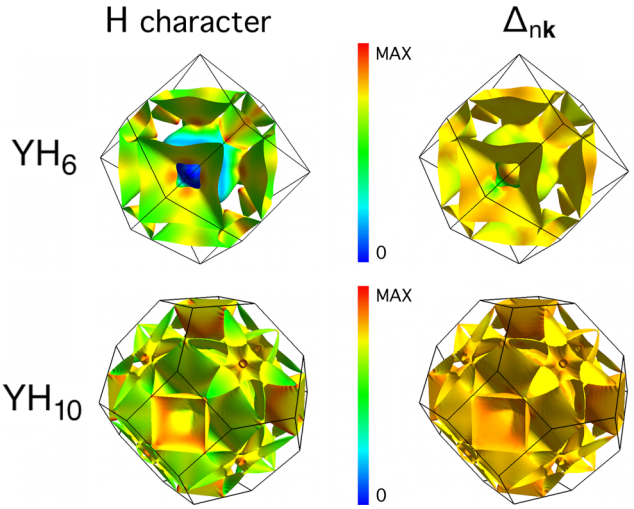

FIG. 3. Fermi surfaces of YH_6 (top row) and YH_{10} (bottom row). In the left panels, the color scale spans the projection onto H states where blue corresponds to 0 and red to 1; in the right panels, it spans the values of the anisotropic gap function at 40 K, blue being 0 meV and red the maximum of 59 (74) meV for YH_6 and YH_{10}, respectively. The band-by-band decomposition (individual Fermi-surface sheets) is available in Sec. II of the Supplemental Material, Tables S3 and S4 [40].

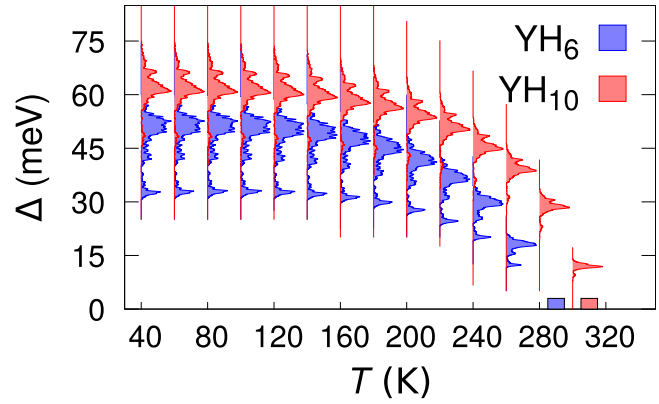

FIG. 4. Energy distribution of the superconducting gap for YH_6 (blue) and YH_{10} (red) as a function of temperature. The rectangles show the extrapolated T_c values.

Before we comment on this figure, let us discuss the main features of the phonon spectra and Coulomb interaction [43–45]. In both YH_6 and YH_{10}, the Eliashberg spectral function (Figs. S3 and S4 in the Supplemental Material [40]) shows a rather uniform distribution of the *e-ph* coupling over all phonons, including the low-energy modes, which are essentially of Y character. Compared to YH_6, the shorter stiffer H-H bonds of YH_{10} translate into 20% larger frequencies for the high-energy bond-stretching modes. The average *e-ph* matrix elements are also higher, leading to a larger *e-ph* coupling in YH_{10} ($\lambda = 2.41$) than in YH_6 ($\lambda = 1.73$). According to our calculations, the Coulomb pseudopotential is the same in both compounds: $\mu^* = 0.11$, resulting from a *GW*-screened Coulomb interaction $\mu_c = 0.11$ and a negligible Morel-Anderson renormalization. This *ab initio* estimate of the Coulomb screening in H clathrates, resulting in a $\mu^* = 0.11$, places these compounds in the same ballpark as most conventional metals. Hence, the anomalously large $\mu^* \simeq 0.22$ invoked in Ref. [23] to reconcile the theoretical estimate with the experimental T_c of the closely related La hydride appears unlikely.

Back to Fig. 3, we observe that, although, in YH_6 and YH_{10}, the distribution of Y and H characters on the Fermi surface is uneven (left panels), this only yields minor ($\pm 10\%$) fluctuations of the superconducting gap around its average value (right). This picture contradicts the idea that SLC hydrides are just a chemical implementation of atomic hydrogen. If that were the case, then the gap should closely track the H-character distribution along the FS. Our calculations show the opposite, indicating that Y-H interorbital interactions are strong [46] as a consequence of the the compact quasi-spherical geometry of the system. Indeed, in SLC, all lattice vibrations modulate the overlap between Y and H orbitals.

We studied the temperature dependence of the superconducting gap by solving the anisotropic ME equations at different temperatures; Fig. 4 displays the temperature evolution of its energy distribution function over the Fermi surface. Well below T_c, i.e., for $T < 80$ K in Fig. 4, this distribution is nearly independent of temperature and shows a broad maximum around 65 meV (55 meV) for YH_{10} (YH_6), originating from the two zone-boundary Fermi surfaces and the two large zone-center Fermi surfaces, plus a smaller tail at lower energies (52 meV for YH_{10} and 36 meV for YH_6) due to the two smallest zone-center Fermi surfaces (see Fig. 3 and Supplemental Material [40]). The gap closes at a critical temperature of 290 K in YH_6 and 310 K in YH_{10} [47]. Since, in both compounds, the dependence of T_c on pressure is very weak as shown in panel (a) of Fig. 5, our predictions for T_c amount to a remarkable agreement with Ref. [14], which, using the *isotropic* Migdal-Eliashberg theory and an empirical value of $\mu^* = 0.10$, estimated 264 K for YH_6 at 120 GPa and 303 K for YH_{10} at 400 GPa.

As shown in panels (b) and (c) of Fig. 5, the weak pressure dependence of T_c results from an almost perfect compensation between the average phonon energy $\omega_{\ln}$, which increases with pressure [48], and the *e-ph* coupling constant λ, which, instead, decreases. For both compounds, this balance approximately holds down to a threshold pressure, below which the lowest optical branch (Γ-L line in YH_{10}, Γ-H line in YH_6) softens, eventually leading to a dynamical instability at $\sim$226 and $\sim$72 GPa, respectively [48]. The soft branch carries a substantial fraction of the total *e-ph* coupling, and a glance at the **q**-dependent electronic susceptibility [48,49] shows that its softening is not due to nesting and must be related to the *e-ph* matrix elements. Interestingly, our frozen-phonon calculations [50,51] show that the anharmonic renormalization of this phonon branch is negligible down to pressures $\leqslant$20 GPa away from the lattice instability [52].

This, in turn, suggests an intrinsic instability of the Y-H system in the SLC structure, which is robust against minor changes in the electronic structure. The common physical origin of the instability of YH_{10} and YH_6 at two very different critical pressures is revealed by their comparison with yet another SLC yttrium hydride: YH_3 (green triangles in Fig. 1),

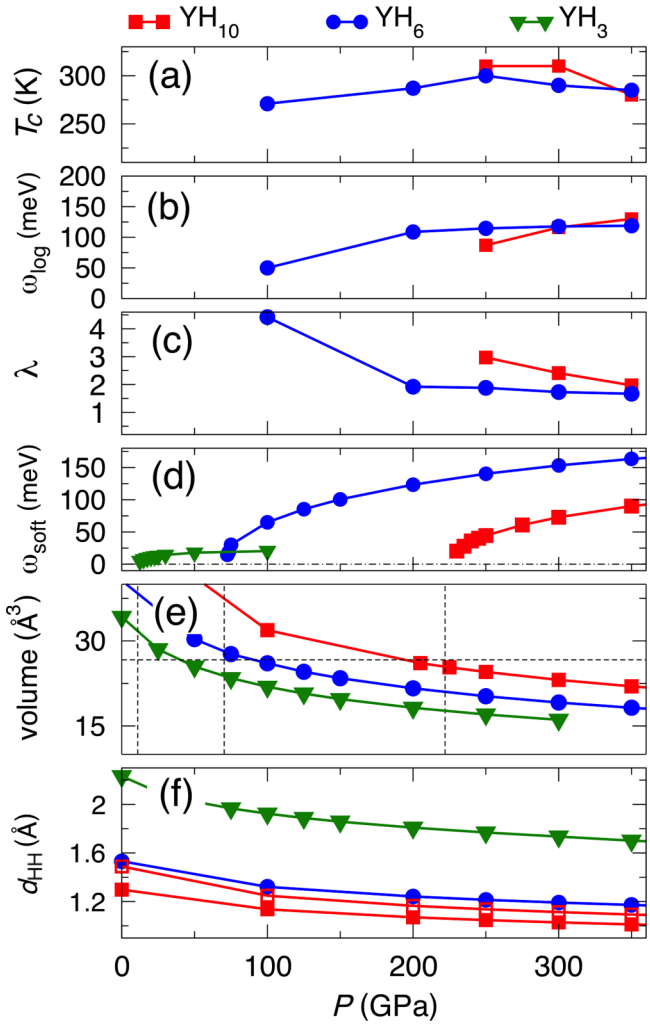

FIG. 5. Behavior of several properties of YH_3 (green triangles), YH_6 (blue circles), and YH_{10} (red squares) as a function of pressure. (a) T_c from anisotropic ME equations ($\mu^* = 0.11$); (b) and (c) Momenta of the *e-ph* spectral function $\alpha^2F(\omega)$, $\omega_{\ln}$ and λ. (d) Frequency of the soft mode. (e) Volume of the polyhedral cage. (f) Nearest-neighbor H-H distance (d_{HH}), see Fig. 1. The dashed lines in (d) and (e) indicate the points where the SLC structures become dynamically unstable.

which, according to our calculations, remains stable down to the much lower pressure of 11.5 GPa [37]. Panel (e) of Fig. 5 shows the V vs P equation of state for the three compounds and clearly evince that the three different pressures below which the soft modes become imaginary in YH_3 (green), YH_6 (blue), YH_{10} (red), correspond to a single volume of $\sim$27 Å^3, which equals the volume of a sphere of radius $\sim$1.9 Å, the covalent radius of Y.

This suggests that, for SLC hydrides with chemical formula XH_n, the minimum stabilization pressure is dictated by the size of the guest atom X: When the hydrogen cage becomes too loose to constrain this atom in its middle, the H lattice breaks down. If this is true, then, for a given atom X, the compounds with larger n (implying denser hydrogen cages with shorter H-H distances) will require higher stabilization pressures. So, as far as the *dynamical stability* is concerned, cages with small n and long H-H distances d_{HH} are preferable because they require lower pressures; on the other hand, in addition to a substantial contribution of the hydrogen electronic and vibrational states to superconductivity, the high-T_c hydrogen superconductivity needs short H-H distances (close to the shortest atomic-solid-hydrogen value of $d_{HH} = 0.98$ Å at 500 GPa) [13,14]; this, on the contrary, calls for large n.

In other words, the competing requirements for dynamical stability and superconductivity together with the different geometrical prefactors which affect the dependence of d_{HH} on the primitive cell/cage volume V [34], provide a natural explanation, pictorially summarized by panels (e) and (f) of Fig. 5, why YH_6 (intermediate cage volume, small d_{HH}) is better than both YH_3 (smallest cage volume, but too large d_{HH}, almost twice than in atomic-solid hydrogen up to 350 GPa) and YH_{10} (smallest d_{HH}, but too large a cage volume).

To summarize, we have studied the superconducting properties of the record high-pressure yttrium hydrides YH_6 and YH_{10} using the first-principles anisotropic Migdal-Eliashberg theory, including Coulomb corrections. Our calculations confirm the prediction of their room-temperature superconductivity [12–14] and reveal that due to the peculiar SLC geometry both anisotropic and anharmonic corrections have a marginal effect on T_c. The Coulomb pseudopotential paramter, computed from first principles within the *GW* approximation, is in line with most conventional superconductors ($\mu^* = 0.11$), in contrast to recent studies which propose a much larger value for related lanthanum SLC hydrides [23]. Besides providing an accurate reference for further work on SLC hydrides, our results may inspire optimization strategies for other superconductors in the same class. A recent work that appeared during the review phase suggests that SLC cages may occur also in ternary hydrides; combining host atoms with different sizes in ternary systems appears a promising route to realize our optimization strategies in practice [53].

This Rapid Communication was supported by the Austrian Science Fund (FWF) Projects No. J 3806-N36 and No. P 30269-N36, the dCluster of the Graz University of Technology, and the VSC3 of the Vienna University of Technology. L.B. and G.B.B. acknowledge support from Fondo Ateneo-Sapienza 2017. L.B. would like to thank A. Sanna for useful discussions on Migdal-Eliashberg theory.

[1] A. P. Drozdov, V. Minkov, S. Besedin, P. Kong, M. Kuzovnikov, D. Knyazev, and M. Eremets, arXiv:1808.07039.

[2] Z. M. Geballe, H. Liu, A. K. Mishra, M. Ahart, M. Somayazulu, Y. Meng, M. Baldini, and R. J. Hemley, Angew. Chem., Int. Ed. **57**, 688 (2018).

[3] M. Somayazulu, M. Ahart, A. K. Mishra, Z. M. Geballe, M. Baldini, Y. Meng, V. V. Struzhkin, and R. J. Hemley, Phys. Rev. Lett. **122**, 027001 (2019).

[4] A. Drozdov *et al.*, Nature **569**, 528 (2019).

[5] A. P. Drozdov, M. I. Eremets, I. A. Troyan, V. Ksenofontov, and S. I. Shylin, Nature (London) **525**, 73 (2015).

[6] D. Duan, Y. Liu, F. Tian, D. Li, X. Huang, Z. Zhao, H. Yu, B. Liu, W. Tian, and T. Cui, Sci. Rep. **4**, 6968 (2014).

[7] N. W. Ashcroft, Phys. Rev. Lett. **21**, 1748 (1968).

[8] N. W. Ashcroft, Phys. Rev. Lett. **92**, 187002 (2004).

[9] D. V. Semenok, I. A. Kruglov, A. G. Kvashnin, and A. R. Oganov, arXiv:1806.00865.

[10] T. Bi, N. Zarifi, T. Terpstra, and E. Zurek, *Reference Module in Chemistry, Molecular Sciences and Chemical Engineering* (Elsevier, Amsterdam, 2018).

[11] H. Wang, J. S. Tse, K. Tanaka, T. Iitaka, and Y. Ma, Proc. Natl. Acad. Sci. USA **109**, 6463 (2012).

[12] Y. Li, J. Hao, H. Liu, J. S. Tse, Y. Wang, and Y. Ma, Sci. Rep. **5**, 9948 (2015).

[13] H. Liu, I. I. Naumov, R. Hoffmann, N. W. Ashcroft, and R. J. Hemley, Proc. Natl. Acad. Sci. USA **114**, 6990 (2017).

[14] F. Peng, Y. Sun, C. J. Pickard, R. J. Needs, Q. Wu, and Y. Ma, Phys. Rev. Lett. **119**, 107001 (2017).

[15] N. Bernstein, C. S. Hellberg, M. D. Johannes, I. I. Mazin, and M. J. Mehl, Phys. Rev. B **91**, 060511(R) (2015).

[16] C. Heil and L. Boeri, Phys. Rev. B **92**, 060508(R) (2015).

[17] J. A. Flores-Livas, A. Sanna, and E. K. Gross, Eur. Phys. J. B **89**, 63 (2016).

[18] I. Errea, M. Calandra, C. J. Pickard, J. Nelson, R. J. Needs, Y. Li, H. Liu, Y. Zhang, Y. Ma, and F. Mauri, Phys. Rev. Lett. **114**, 157004 (2015).

[19] A. P. Drozdov, M. I. Eremets, and I. A. Troyan, arXiv:1508.06224.

[20] J. A. Flores-Livas, M. Amsler, C. Heil, A. Sanna, L. Boeri, G. Profeta, C. Wolverton, S. Goedecker, and E. K. U. Gross, Phys. Rev. B **93**, 020508 (2016).

[21] A. Shamp, T. Terpstra, T. Bi, Z. Falls, P. Avery, and E. Zurek, J. Am. Chem. Soc **138**, 1884 (2016).

[22] Y. Fu, X. Du, L. Zhang, F. Peng, M. Zhang, C. J. Pickard, R. J. Needs, D. J. Singh, W. Zheng, and Y. Ma, Chem. Mater. **28**, 1746 (2016).

[23] I. A. Kruglov, D. V. Semenok, H. Song, Radosław Szczęśniak, I. A. Wrona, R. Akashi, M. M. D. Esfahani, D. Duan, T. Cui, A. G. Kvashnin, and A. R. Oganov, arXiv:1810.01113.

[24] L. Liu, C. Wang, S. Yi, K. W. Kim, J. Kim, and J.-H. Cho, Phys. Rev. B **99**, 140501(R) (2019).

[25] H. Liu, I. I. Naumov, Z. M. Geballe, M. Somayazulu, J. S. Tse, and R. J. Hemley, Phys. Rev. B **98**, 100102(R) (2018).

[26] J. M. McMahon and D. M. Ceperley, Phys. Rev. B **84**, 144515 (2011).

[27] M. Borinaga, I. Errea, M. Calandra, F. Mauri, and A. Bergara, Phys. Rev. B **93**, 174308 (2016).

[28] C. M. Pépin, G. Geneste, A. Dewaele, M. Mezouar, and P. Loubeyre, Science **357**, 382 (2017).

[29] C. Heil, G. B. Bachelet, and L. Boeri, Phys. Rev. B **97**, 214510 (2018).

[30] Our density functional theory (DFT) calculations are carried out in the generalized gradient approximation [54]. We employed the QUANTUM ESPRESSO package [55] for the electronic structure and lattice dynamics, the EPW code [32] for the electron-phonon interaction and the superconducting gap, the WANNIER90 code for generating maximally localized Wannier functions [56], and the STERNHEIMERGW code [41,42] for the screened Coulomb interaction. Details on the choice of pseudopotential [57,58], **k**-space integration, etc., can be found in Sec. I of the Supplemental Material [40].

[31] E. R. Margine and F. Giustino, Phys. Rev. B **87**, 024505 (2013).

[32] S. Poncé, E. R. Margine, C. Verdi, and F. Giustino, Comput. Phys. Commun. **209**, 116 (2016).

[33] In this Rapid Communication, we do not consider the related SLC structure of YH_9 predicted in Ref. [14] because, according to our calculations, it is dynamically unstable.

[34] See Sec. II of the Supplemental Material for details on the crystal structure of all compounds studied in this Rapid Communication [40].

[35] A. Machida, A. Ohmura, T. Watanuki, K. Aoki, and K. Takemura, Phys. Rev. B **76**, 052101 (2007).

[36] D. Y. Kim, R. H. Scheicher, and R. Ahuja, Phys. Rev. Lett. **103**, 077002 (2009).

[37] Although. in this Rapid Communication, we only address its dynamical stability, for completeness, we recalculated the critical temperature of YH_3 at several pressures. Our results are in very good agreement with those of Ref. [36], which predicted a maximum T_c of 40 K at 20 GPa, followed by a low-T_c region at higher pressures.

[38] S. di Cataldo, C. Heil, G. B. Bachelet, and L. Boeri (unpublished).

[39] A band-by-band breakdown of the Fermi surface is provided in Tables S3 and S4 of the Supplemental Material [40].

[40] The Supplemental Material is available at https://link.aps.org/supplemental/10.1103/PhysRevB.99.220502 for more details.

[41] F. Giustino, M. L. Cohen, and S. G. Louie, Phys. Rev. B **81**, 115105 (2010).

[42] H. Lambert and F. Giustino, Phys. Rev. B **88**, 075117 (2013).

[43] A. B. Migdal, Sov. Phys. JETP **34**, 996 (1958).

[44] G. M. Eliashberg, Sov. Phys. JETP **11**, 696 (1960).

[45] See the Supplemental Material [40] for more details, including a band-by-band decomposition of the H vs Y characters, gap, and Coulomb pseudopotential. Detailed plots of the phonon dispersions, *e-ph* spectral functions, and wave-vector-resolved depictions of the Coulomb potential $\mu_{\mathbf{k}}$ are also provided in the Supplemental Material [40].

[46] H. Suhl, B. T. Matthias, and L. R. Walker, Phys. Rev. Lett. **3**, 552 (1959).

[47] The McMillan-Allen-Dynes values [59] are much smaller: $T_c =$ 225 K in YH_{10} and $T_c = 185$ K in YH_6 due to the well-known underestimation of T_c for large values of λ.

[48] See Sec. V of the Supplemental Material [40] for details on the phonon dispersions and *e-ph* coupling functions.

[49] C. Heil, H. Sormann, L. Boeri, M. Aichhorn, and W. von der Linden, Phys. Rev. B **90**, 115143 (2014).

[50] P. K. Lam and M. L. Cohen, Phys. Rev. B **25**, 6139 (1982).

[51] F. Giustino, *Materials Modelling Using Density Functional Theory: Properties and Predictions* (Oxford University Press, Oxford, 2014).

[52] See Sec. VI of the Supplemental Material [40] for details on anharmonicity in YH_6 and YH_{10}.

[53] X. Liang, A. Bergara, L. Wang, B. Wen, Z. Zhao, X.-F. Zhou, J. He, G. Gao, and Y. Tian, Phys. Rev. B **99**, 100505(R) (2019).

[54] J. P. Perdew, K. Burke, and M. Ernzerhof, Phys. Rev. Lett. **77**, 3865 (1996).

[55] P. Giannozzi, S. Baroni, N. Bonini, M. Calandra, R. Car, C. Cavazzoni, D. Ceresoli, G. L. Chiarotti, M. Cococcioni, I. Dabo, A. D. Corso, S. d. Gironcoli, S. Fabris, G. Fratesi,

R. Gebauer, U. Gerstmann, C. Gougoussis, A. Kokalj, M. Lazzeri, L. Martin-Samos, N. Marzari, F. Mauri, R. Mazzarello, S. Paolini, A. Pasquarello, L. Paulatto, C. Sbraccia, S. Scandolo, G. Sclauzero, A. P. Seitsonen, A. Smogunov, P. Umari, and R. M. Wentzcovitch, J. Phys.: Condens. Matter **21**, 395502 (2009).

[56] A. A. Mostofi, J. R. Yates, Y.-S. Lee, I. Souza, D. Vanderbilt, and N. Marzari, Comput. Phys. Commun. **178**, 685 (2008).

[57] D. R. Hamann, Phys. Rev. B **88**, 085117 (2013).

[58] M. Schlipf and F. Gygi, Comput. Phys. Commun. **196**, 36 (2015).

[59] P. B. Allen and R. C. Dynes, Phys. Rev. B **12**, 905 (1975).